ERRATUM POSTED 24 NOVEMBER 2023

HUMAN GENETICS

Abrogation of MAP4K4 protein function causes congenital anomalies in humans and zebrafish

Victoria Patterson[1,2], Farid Ullah[3], Laura Bryant[4], Dong Li[5], John N. Griffin[6], Alpa Sidhu[7], Sheila Saliganan[8], Mackenzie Blaile[9], Margarita S. Saenz[9], Rosemarie Smith[10], Sara Ellingwood[10], Dorothy K. Grange[11], Xuyun Hu[12], Maimaiti Mireguli[13], Yanfei Luo[13], Yiping Shen[14,15], Maureen Mulhern[16], Elaine Zackai[4], Alyssa Ritter[4], Kosuke Izumi[4], Julia Hoefele[17], Matias Wagner[17,18,19], Korbinian M. Riedhammer[17,20], Barbara Seitz[21], Nathaniel H. Robin[22], Dana Goodloe[22], Cyril Mignot[23], Boris Keren[24], Helen Cox[24], Joanna Jarvis[24], Maja Hempel[25], Cynthia Forster Gibson[26], Frederic Tran Mau-Them[27], Antonio Vitobello[28,29], Ange-Line Bruel[27], Arthur Sorlin[27], Sarju Mehta[30], F. Lucy Raymond[31], Kelly Gilmore[32], Bradford C. Powell[33], Karen Weck[34], Chumei Li[35], Anneke T. Vulto-van Silfhout[36], Thea Giacomini[37], Maria Margherita Mancardi[38], Andrea Accogli[39,40], Vincenzo Salpietro[41], Federico Zara[41], Neeta L. Vora[32], Erica E. Davis[3], Rebecca D. Burdine[1]*, Elizabeth Bhoj[4]*

We report 21 families displaying neurodevelopmental differences and multiple congenital anomalies while bearing a series of rare variants in *mitogen-activated protein kinase kinase kinase kinase 4* (*MAP4K4*). MAP4K4 has been implicated in many signaling pathways including c-Jun N-terminal and RAS kinases and is currently under investigation as a druggable target for multiple disorders. Using several zebrafish models, we demonstrate that these human variants are either loss-of-function or dominant-negative alleles and show that decreasing Map4k4 activity causes developmental defects. Furthermore, MAP4K4 can restrain hyperactive RAS signaling in early embryonic stages. Together, our data demonstrate that MAP4K4 negatively regulates RAS signaling in the early embryo and that variants identified in affected humans abrogate its function, establishing *MAP4K4* as a causal locus for individuals with syndromic neurodevelopmental differences.

INTRODUCTION

The RAS signaling pathway is one of many signaling cascades used throughout development to sculpt the growing embryo. The RAS pathway is activated by ligand binding to a receptor tyrosine kinase (RTK), which ultimately leads to a signaling cascade involving the sequential phosphorylation of RAS, rapidly accelerated fibrosarcoma, mitogen-activated protein kinase (MAPK) kinase (MEK) and extracellular signal–regulated kinase (ERK). Many proteins are directly involved in the transduction of signals, and many more act to positively or negatively modulate pathway activity (*1*).

While RAS signaling helps direct cell survival, growth, and differentiation in the healthy state, aberrations in signaling can cause disease. Loss of signaling is embryonically lethal, but variants in RAS, or other pathway components, that lead to hyperactive RAS signaling are a common cause of cancer (*2*, *3*). These activating variants generally arise in somatic cells, but when such variants are inherited through the germ line, they cause a group of developmental syndromes collectively known as RASopathies (*4*, *5*). Although each RASopathy is clinically distinct, there is substantial overlap in the symptoms observed in affected individuals (*6*, *7*). Particularly common are craniofacial anomalies (CFAs), congenital heart defects (CHDs), developmental delay (DD), short stature, and a predisposition to developing cancer. Although some RASopathy syndromes are rare, others are more common and collectively RASopathies occur in one of 1000 births (*5*).

Many RASopathy-associated genes have been identified, and the precise pathway disruption dictates the clinical presentation of the disease (*6*, *7*). For example, disease-causing variants in *MEK* cause cardiofaciocutaneous syndrome, while disease-causing variants in *NRAS*, *RAF1*, and others are associated with Noonan syndrome. Still, many affected individuals lack a molecular diagnosis following exome or genome sequencing, and many presumably carry variants in genes not previously associated with human disease. Identifying and validating pathogenic variants in candidate genes causing RASopathy phenotypes in a multicenter cohort provides an opportunity to discover regulators of RAS signaling while potentially providing targets for therapeutic intervention in both the cases under study, and larger RAS-related conditions.

MAPK kinase kinase kinase 4 (*MAP4K4*) encodes a Ste20 family serine/threonine protein kinase, which contains a kinase domain, an interdomain, and a citron homology (CNH) domain (*8*, *9*). The interdomain and CNH domain mediate binding to interaction partners, with the CNH domain having an additional role in regulating kinase activity (*10*, *11*). MAP4K4 is expressed in all tissues, although expression is highest in brain and testes, and five isoforms have been isolated (*12*). Loss of MAP4K4 disrupts embryonic development (*13*–*16*), whereas elevated protein levels have been implicated in diseases including cancer, atherosclerosis, and diabetes (*12*, *17*–*28*). While MAP4K4 has been implicated in several signaling pathways, the protein has been reported to have a role in regulating RAS signaling (*13*, *29*–*31*).

Here, we report a cohort of 26 affected individuals from 21 unrelated families with neurodevelopmental differences, cardiac issues, and CFAs who share a phenotype overlap with RASopathies and harbor a series of rare variants in *MAP4K4*. We use a zebrafish model to demonstrate that these variants reduce MAP4K4 function.

Some of the variants work through either a loss of function (LOF) or dominant negative (DN) in nature. We show that increasing or decreasing MAP4K4 activity causes similar developmental defects in zebrafish embryos. Last, we demonstrate that MAP4K4 can restrain hyperactive RAS signaling in early zebrafish embryos. Together, our data demonstrate that MAP4K4 is a negative regulator of RAS signaling in the context of the early embryo and that variants identified in affected humans abrogate its function, releasing inhibition of RAS signaling. This work establishes an association of variants in *MAP4K4* with features that overlap other RASopathy syndromes.

RESULTS

Individuals with rare variants in *MAP4K4* display neurodevelopmental differences and congenital anomalies

Exome sequencing of an affected female diagnosed with Noonan-like syndrome identified a c.2591T>A;p.Leu864Ter variant in *MAP4K4* (GenBank identifier: NM_001242559.1), which was absent from ~123,350 individuals in the genome aggregation database [The Genome Aggregation Database (gnomAD) v2.1.1] and had a probability of LOF intolerance of 1 and missense *z* score of 4.74. The affected individual displayed dysmorphic craniofacial features, limb abnormalities, pulmonary artery stenosis, intellectual disability (ID) and DD, and behavioral disorders (table S1). Sequencing of family members revealed that the variant was present in the proband's mother and sibling. Both mother and sibling presented with mild ID/DD, and the sibling displayed CFA. There were no other *MAP4K4* variants of interest identified in the remaining affected individuals in this original discovery cohort.

A LOF de novo variant in *MAP4K4* (p.Gln1157Ter) was previously reported in a fetus with a complex CHD and congenital abnormalities of the kidneys and urinary tract. The functional impact of this change was not assayed, but the locus was considered a candidate disease-causing gene (*32*). Through international collaboration, including via GeneMatcher (*33*), we identified 26 individuals from 21 unrelated families with heterozygous variants in *MAP4K4* (Table 1 and table S1). Two missense variants (p.Gly173Asp and p.Arg152Trp) are recurrent and have arisen de novo in two families each, yielding an allelic series of 19 variants; eight truncating, nine missense, and two intronic splice site variants (Fig. 1, A and B). These variants were not detected in gnomAD, and either arose de novo, or were inherited from an affected parent. Some parents were unavailable for testing to determine inheritance. Individuals harboring *MAP4K4* variants display a high incidence of DD (80%), ID (42%), and short stature (40%). Variable symptoms include CFA (up to 29%), CHD (27%), hypotonia (25%), limb abnormalities (29%), micrognathia (29%), posteriorly rotated ears (29%), attention deficit disorder (30%), central nervous system structural defects (31%), and fetal finger pads (19%) (Fig. 2 and Table 1). Although the clinical presentation of affected individuals is varied, most display symptoms of neurodevelopmental conditions with a constellation of features overlapping those observed in patients with RASopathies. These data are consistent with the previously reported role for MAP4K4 in regulating RAS signaling.

Truncation of MAP4K4 abrogates protein function

To determine the effect of *MAP4K4* variants on protein function, we used zebrafish to conduct rapid screening. We generated an expression construct encoding human MAP4K4 and performed site-directed mutagenesis to introduce seven randomly selected variants identified in cases; five truncating and two missense variants. The annotation of the variants differs between the protein encoded by the patient reference sequence (NM_001242559.1) and the expression construct (*34*). However, the context of the affected residues within the overall sequence is maintained (Fig. 1A).

Zebrafish embryos were injected at the one-cell stage with mRNA encoding either wild-type (WT) or variant *MAP4K4* at equivalent doses across conditions. $MAP4K4^{WT}$ expression causes a range of developmental defects by 3 days post fertilization (dpf). Larvae had a shorter body length compared to vehicle-injected controls and displayed CFA, cardiac edema indicative of heart defects, hydrocephaly, small or malformed eyes, yolk extension defects, and curved body axes (Fig. 3A). These phenotypes occurred in any and all combinations. Notably, ectopic human *MAP4K4*

[1]Princeton University, Princeton, NJ 08544, USA. [2]Department of Biology, University of York, York, UK. [3]Stanley Manne Children's Research Institute, Ann & Robert H. Lurie Children's Hospital of Chicago, Departments of Pediatrics and Cell and Developmental Biology, Feinberg School of Medicine, Northwestern University, Chicago, IL 60611, USA. [4]Children's Hospital of Philadelphia, Philadelphia, PA 19104, USA. [5]Center for Applied Genomics, Children's Hospital of Philadelphia, Philadelphia, PA, USA. [6]University of East Anglia, Norwich Research Park, Norwich NR4 7TJ, UK. [7]The Stead Family Department of Pediatrics, University of Iowa Hospitals and Clinics, Iowa City, IA 52242, USA. [8]Ambry Genetics, 1 Enterprise, Aliso Viejo, CA 92656, USA. [9]University of Colorado Anschutz Medical Campus, 13001 E 17th Pl, Aurora, CO 80045, USA. [10]Maine Medical Center, 22 Bramhall St, Portland, ME 04102, USA. [11]St. Louis Children's Hospital, Washington University School of Medicine, 660 S Euclid Ave, St. Louis, MO 63110, USA. [12]Beijing Key Laboratory for Genetics of Birth Defects, Beijing Pediatric Research Institute, MOE Key Laboratory of Major Diseases in Children, Genetics and Birth Defects Control Center, Beijing Children's Hospital, Capital Medical University, National Center for Children's Health, Beijing, China. [13]First Affiliated Hospital of Xinjiang Medical University, Department of Pediatrics, Xinjiang Uygur Autonomous Region, China. [14]Boston Children's Hospital, Harvard Medical School, Boston, MA 02115, USA. [15]Maternal and Child Care Hospital of Guangxi Zhuang Autonomous Region, Guangxi, Nanning, China. [16]Columbia University Irving Medical Center, 630 W. 168th St, New York, NY 10032, USA. [17]Institute of Human Genetics, Klinikum rechts der Isar, School of Medicine, Technical University of Munich, Munich, Germany. [18]Institute of Neurogenomics, Helmholtz Zentrum München, Neuherberg, Germany. [19]Department of Pediatrics, Division of Pediatric Neurology, Developmental Medicine and Social Pediatrics, University Hospital of Munich, Ludwig Maximilians University, Munich, Germany. [20]Department of Nephrology, Klinikum rechts der Isar, School of Medicine, Technical University of Munich, Munich, Germany. [21]KfH Pediatric Kidney Center Munich, Munich, Germany. [22]University of Alabama at Birmingham, 1720 University Blvd, Birmingham, AL 35233, USA. [23]APHP-Sorbonne Université, GH Pitié-Salpêtrière, Paris, France. [24]Clinical Genetics Unit, Birmingham Women's and Children's NHS Foundation Trust, Mindelsohn Way, Birmingham B15 2TG, UK. [25]University Hospital Hamburg-Eppendorf, Martinistraße 52, 20251 Hamburg, Germany. [26]Trillium Health Partners, Mississauga, ON L5B 2V2, Canada. [27]University of Bourgogne, Dijon, France. [28]UMR1231 GAD, Inserm, Université Bourgogne-Franche-Comté, Dijon, France. [29]Unité Fonctionnelle Innovation en Diagnostic génomique des maladies rares, FHU-TRANSLAD, CHU Dijon Bourgogne, Dijon, France. [30]Addenbrooke's Hospital, Cambridge, UK. [31]University of Cambridge, Cambridge, UK. [32]Department of Ob/Gyn, Division of Maternal-Fetal Medicine, University of North Carolina at Chapel Hill, Chapel Hill, NC 27599, USA. [33]Department of Genetics, University of North Carolina at Chapel Hill, Chapel Hill, NC 27599, USA. [34]Department of Pathology and Laboratory Medicine, University of North Carolina at Chapel Hill, Chapel Hill, NC 27599, USA. [35]McMaster University, 1280 Main St W, Hamilton, ON L8S 4L8, Canada. [36]Radboudumc Nijmegen, 6500 HB Nijmegen, Netherlands. [37]Unit of Child Neuropsychiatry, University of Genova, EpiCARE Network, IRCCS Istituto Giannina Gaslini, Genova, Italy. [38]Unit of Child Neuropsychiatry, EpiCARE Network, IRCCS Istituto Giannina Gaslini, Genova, Italy. [39]Division of Medical Genetics, Department of Medicine, McGill University Health Centre, Montreal, QC, Canada. [40]Department of Human Genetics, McGill University, Montreal, QC, Canada. [41]Department of Biotechnological and Applied Clinical Science, University of L'Aquila, 67100 L'Aquila, Italy.
*Corresponding author. Email: rburdine@princeton.edu (R.D.B.); bhoje@chop.edu (E.B.)

Table 1. Clinical features in 27 individuals with heterozygous *MAP4K4* variants. The most common features are developmental delay (DD), intellectual disability (ID), attention deficit disorder, abnormal brain magnetic resonance imaging (MRI), and short stature. M, male; F, female; Unk, unkown.

Individual gender	13 M/12 F/1 Unk
Age range	0–40 years
Clinical findings:	
Short stature	8/20 (40%)
Frontal bossing	4/21 (19%)
Cranial abnormality	4/21 (19%)
Ocular hypertelorism	3/21 (14%)
Arched eyebrows	3/21 (14%)
High/broad nasal bridge	4/21 (19%)
Anteverted nares	5/21 (24%)
Long philtrum	6/21 (29%)
Micrognathia	6/21 (29%)
Down-slanted palpebral fissures	6/21 (29%)
Median nose tip groove	2/21 (10%)
Posteriorly rotated ears	6/21 (29%)
Preauricular pits/tags	2/21 (10%)
Cleft lip	0/19 (0%)
Cleft palate	1/21 (5%)
Webbed neck	2/21 (10%)
Limb abnormalities	6/21 (29%)
Wide nipples	6/21 (27%)
Pectus excavatum	3/21 (14%)
Hemangiomas	2/21 (10%)
Digestive anomaly	4/21 (19%)
Congenital heart defect	6/22 (27%)
Umbilical hernia/omphalocele	1/21 (5%)
Anorectal malformations	1/21 (5%)
Small broad hands	3/21 (14%)
Clinodactyly	4/21 (19%)
Fetal finger pads	4/21 (19%)
Renal anomaly	4/21 (19%)
Abnormal brain MRI	5/16 (31%)
Hearing loss	1/21 (5%)
DD	16/20 (80%)
ID	8/21 (42%)
Age first sitting	Range: 6 months to 12 years
Age first walking	Range: 10 months to 3 years
Age first words	Range: 12 months to 5 years
Autism	3/18 (17%)
Attention deficit disorder	6/20 (30%)
Seizures	6/22 (27%)
Hypotonia	5/20 (25%)

mRNA is introduced to a WT background, in which endogenous *map4k4* is expressed starting from zygotic stages and continuing at least through larval day 5 (Expression Atlas: www.ebi.ac.uk/gxa/experiments/E-ERAD-475). Hence, this assay does not recapitulate affected human phenotype; rather, it allows assessment of the effect of WT protein on development for comparison to variant protein.

We assessed the impact of *MAP4K4* variants on morphology. An equivalent dose of mRNA bearing case-associated variants affected the same tissues as $MAP4K4^{WT}$, albeit with varying severity (Fig. 3A). Larvae were scored for body defects (Fig. 3B), including truncations, and lateral or dorsoventral curvatures. All variants except $MAP4K4^{P232X}$ significantly increased the incidence of body defects, with the greatest effects observed for $MAP4K4^{R152W}$ and the least effect measured for $MAP4K4^{L889X}$. A similar trend was observed for the other three classes of defects; eye defects, including small eyes and malformations such as coloboma; heart defects, evidenced by pericardial edema; and yolk defects, observed as anteroposterior shortening or dorsoventral thickening of the yolk extension or absence of the yolk constriction (Fig. 3, C to E). We also measured body length (Fig. 3F) and detected a similar trend, with some variants having little effect on body length, while others greatly reduced the length of embryos, as does ectopic expression of $MAP4K4^{WT}$.

A subset of larvae expressing *MAP4K4* variants appeared to have CFA at 3 dpf, with the eyes appearing more anteriorly positioned compared to controls. Because CFA was observed in our human cohort with *MAP4K4* variants, we next examined craniofacial development at 5 dpf, using Alcian blue stain to visualize the cartilage (Fig. 4A). We measured the distance between the Meckel's and ceratohyal cartilages at the midline as a proxy for jaw length. Expression of $MAP4K4^{WT}$ reduced the length of the jaw (Fig. 4B), as did most variants, although to varying extents. The incidence of CFA was also increased, with expression of *MAP4K4* variants causing misshapen or misplaced cartilages (Fig. 4C). In extreme cases, the cartilage developed bilaterally instead of medially, possibly due to aberrant neural crest cell migration.

For all the developmental structures assayed, the five truncation variants had the least effect upon development. The missense variants, $MAP4K4^{R152W}$ and $MAP4K4^{G173D}$, were the most disruptive. Because $MAP4K4^{WT}$ disrupted larval development, this indicates that the truncation variants reduce MAP4K4 function, such that it no longer hinders development in the same way as ectopic expression of $MAP4K4^{WT}$ does. While this finding supports the fact that loss of MAP4K4 function underlies disease in cases with frameshift variants, it does not explain how missense variants may lead to disease in the remainder of our cohort.

Missense variants have DN effects

To address whether missense variants may confer a DN effect, we examined the effect of introducing a known DN version of the protein, $MAP4K4^{D153N}$ (Figs. 3 and 4). This variant is a kinase-dead variant that is capable of interfering with the endogenously expressed Map4k4 protein, effectively knocking down protein function (*10*). Expression of $MAP4K4^{D153N}$ caused an increase in embryonic abnormalities of all classes and reduced the length of both body and jaw. In most cases, the measured effect is similar to or greater than that of expressing $MAP4K4^{WT}$, suggesting that decreasing Map4k4 function has a similar impact to increasing it

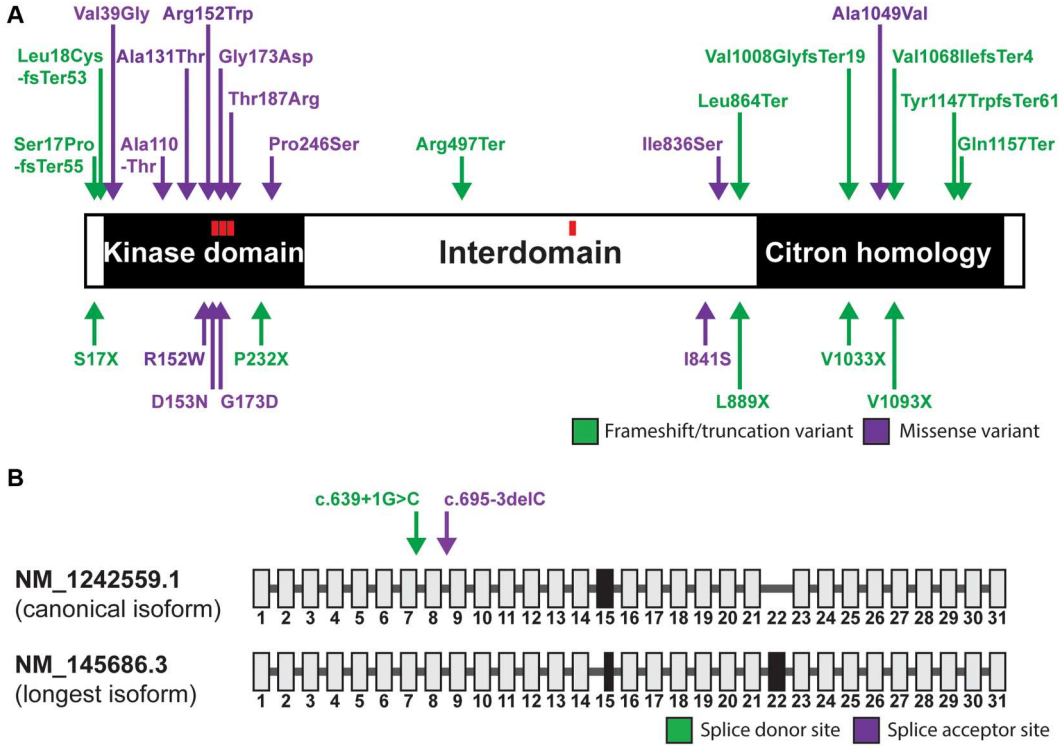

Fig. 1. MAP4K4 variants identified in affected individuals cluster in functional domains. (**A**) A schematic of the mitogen-activated protein kinase kinase kinase kinase 4 (MAP4K4) protein is shown (NP_001229488.1), with the positions of variants identified in our cohort indicated by arrows above the diagram. Green arrows represent frameshift or truncation variants, and purple arrows represent missense variants. Arrows below the diagram represent the corresponding mutations introduced to our expression construct (NM_001384485.1, Δ2078-2083). Regions reported to be phosphorylated are shown by red squares. (**B**) A schematic of the canonical transcript and a longer isoform are shown. Gray boxes represent exons conserved between sequences, and black boxes represent exons that differ between sequences. Green arrows represent variants in splice donor sites, and purple arrows represent variants in splice acceptor sites.

by supplying exogenous *MAP4K4*. We therefore hypothesized that a subset of the missense variants that we observed to have similar effects to $MAP4K4^{WT}$ in our assays may represent DN hypomorphic alleles.

Because our patient cohort was composed of individuals displaying overlap with the clinical features of RASopathy syndromes, we expect that disease etiology will arise from modulation of the RAS signaling pathway. Previous work has demonstrated that modulating the RAS pathway in zebrafish affects the aspect ratio of embryos at 11 hours post fertilization (hpf) (*35*–*44*). Pathway activation by expressing hyperactive RASopathy-associated *MEK* or *BRAF* variants causes embryo elongation, while pharmacological inhibition of MEK shortens the embryo (*35*). Furthermore, the extent of elongation or shortening correlates with the strength of pathway activation (*44*). We predicted that if MAP4K4 modulates RAS signaling, then this assay would allow us to distinguish between four allele types; compared to $MAP4K4^{WT}$, DN variants should have an opposing effect on the aspect ratio, LOF variants should have no effect, hypomorphic alleles should have a similar effect but to a lesser degree, and gain-of-function variants should cause an effect greater than $MAP4K4^{WT}$.

Overexpression of $MAP4K4^{WT}$ significantly reduced the aspect ratio at 11 hpf (Fig. 5A). This indicates that the signaling pathway is inhibited upon increasing the amount of functional protein. Introducing $MAP4K4^{D153N}$ leads to elongation of the embryo, consistent with hyperactivation of the signaling pathway as a result of losing Map4k4 function. Together, these data demonstrate that MAP4K4 acts as a negative regulator of RAS signaling in this context.

We next assessed the impact of variants on the aspect ratio. Ectopic expression of variant *MAP4K4* mRNA either had little effect or caused embryo elongation (Fig. 5A), allowing us to group variants as either DN or LOF. DN variants—$MAP4K4^{R152W}$, $MAP4K4^{G173D}$, and $MAP4K4^{V1033X}$—increased the aspect ratio, although not as strongly as the $MAP4K4^{D153N}$ variant. The remaining variants—$MAP4K4^{S17X}$, $MAP4K4^{P232X}$, $MAP4K4^{L889X}$, and $MAP4K4^{V1093X}$—had no effect on the aspect ratio. These variants were designated as LOF, since they neither exerted an additive effect like combining $MAP4K4^{WT}$ and endogenous Map4k4 nor interfered with the function of endogenous Map4k4, as does $MAP4K4^{D153N}$. Thus, all the variants detected in patients reduce protein function, with a subset capable of further interfering with the function of WT alleles.

We also tested a variant that is not present in humans, $MAP4K4^{I841S}$, but resulted from plasmid mutagenesis. This variant retained enough function to reduce the aspect ratio compared to vehicle-injected controls, but not to the same extent as $MAP4K4^{WT}$. Thus, we concluded that p.Ile841Ser is a hypomorphic allele. Although not directly relevant to our human cohort, this serendipitous result demonstrates that we can distinguish between hypomorphic and LOF alleles with this assay. The expression of hypomorphic *MAP4K4* represents an intermediate state between

Fig. 2. Affected individuals display CFAs and limb abnormalities. (**A** to **D**) Affected individual at the age of 4 months (A), 14 months (B), and 28 years (C and D). Individual displays ptosis, high arched eyebrows, broad nasal root, thin lips, and posteriorly rotated ears. (**E** to **H**) Affected mother at 29 years of age (E and F) and her affected child (G and H) at 11 months of age. Individuals display down-slanting palpebral fissures, low-set ears, and thin upper lip. (**I**) Affected individual at 18 years of age. Individual displays high anterior hairline, ptosis, and down-slanting palpebral fissures. (**J** to **L**) Affected infant displays asymmetric crying facies, wide and flat nasal bridge, posteriorly rotated ears, as well as shoulder, hand, and elbow malformations. (**M** to **P**) Affected individuals display limb abnormalities including brachydactyly (M to O) and wrist contractures (P).

overexpression of WT and LOF variants, and analysis of the later phenotypes show a phenotype that is similar to but weaker than that caused by overexpression of *MAP4K4*^{WT} (Figs. 3 and 4). This supports our earlier conclusion that either increasing or decreasing endogenous protein function disrupts development similarly, with LOF alleles producing modest phenotypic consequences.

Both increasing and decreasing MAP4K4 function causes similar phenotypes

To compare the phenotypic output induced by ectopic expression of *MAP4K4* across variants, we performed hierarchical clustering (Fig. 5B). Clustering analysis ranked the DN *MAP4K4*^{D153N} and *MAP4K4*^{R152W} and the hypomorphic *MAP4K4*^{I815S} as being more similar to *MAP4K4*^{WT} than to the weaker DN variants or LOF alleles. Thus, these aggregate data suggest that either increasing or decreasing the amount of functional *MAP4K4* leads to similar phenotypic output in a developmental context.

Consistent with this hypothesis, treating zebrafish embryos with the MAP4K4 inhibitor PF06260933 to deplete endogenous Map4k4 caused developmental defects in a dose-responsive manner. Larvae exhibited cardiac edema, small eyes, and yolk malformations at 3 dpf as well as CFA at 5 dpf (Fig. 6, A and B). The incidence of abnormal embryos is increased upon exposure to higher doses of inhibitor (Fig. 6C), while both body and jaw lengths are shortened by

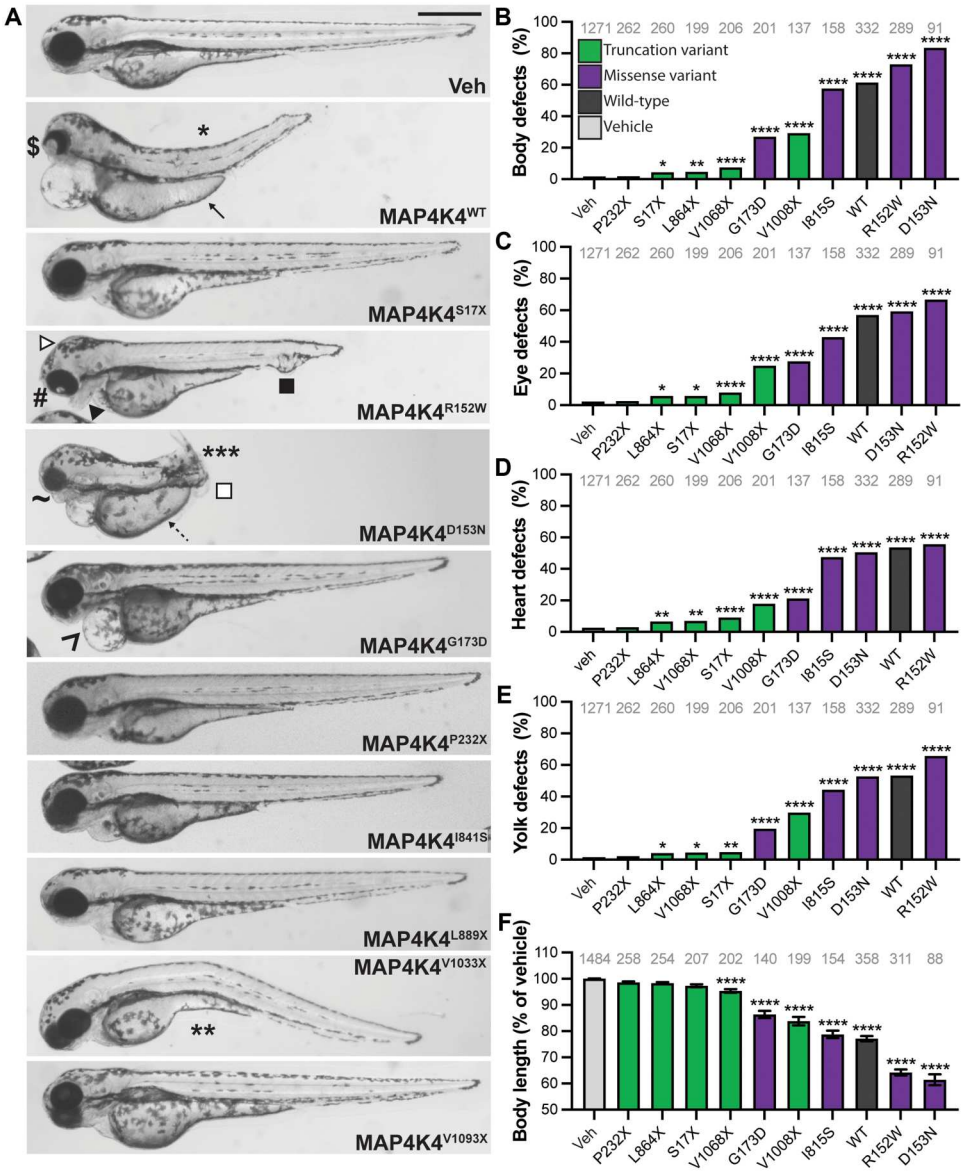

Fig. 3. *MAP4K4* variants cause LOF. (**A**) Larvae microinjected with variant *MAP4K4* were imaged at 3 days post fertilization (dpf); representative lateral views are shown. Ectopic expression of *MAP4K4* caused developmental defects, including craniofacial anomalies (CFAs; closed arrowhead), hydrocephaly (white arrowhead), and cloacal defects (closed square). Larvae are arranged according to the position of the variant within the protein (top to bottom; N to C terminus). (**B** to **E**) Developmental defects were quantified as a percentage of total larvae displaying the defect. (B) Body defects included dorsal (*), ventral (**) and lateral (***) curvatures, and truncations (white square). (C) Eye defects included coloboma ($), cyclopia (#), and small eyes (~). (D) Heart defects included pericardial edema (^). (E) Yolk defects included thickening of the yolk extension (solid arrow) and absent yolk constriction (dashed arrow). (**F**) Body length was measured and normalized to the average of the vehicle-injected siblings (Veh) and is reduced by expression of $MAP4K4^{WT}$ and missense variants but is less affected by truncation variants. Scale bar, 500 μm (A). Graphs (B to F): pale gray, vehicle; dark gray, $MAP4K4^{WT}$; purple, missense variants; and green, truncation variants. $^*P < 0.05$; $^{**}P < 0.01$; $^{***}P < 0.001$; $^{****}P < 0.0001$ by pairwise chi-square test (B to E) or Student's *t* test (F) compared to vehicle. Analysis of variance (ANOVA) gives $P < 0.0001$ for (F). *n* numbers are inset to graphs in gray text. Error bars represent SEM. WT, wild type.

drug treatment (Fig. 6, D and E). These phenotypes are highly reminiscent of those observed for embryos that overexpress *MAP4K4*.

To corroborate the observations from MAP4K4 pharmacological inhibition, we performed ablation of the endogenous *map4k4* transcript. We obtained a splice blocking morpholino (MO) targeting the exon 13 donor site, validated exon skipping by reverse transcription polymerase chain reaction (RT-PCR) of embryos injected with either 6 or 9 ng of MO, and performed cloning and sequencing to confirm the excision of 73 base pairs to induce a frameshift and premature truncation (fig. S1, A to C). Next, we assessed the mandibular phenotype of larvae injected with increasing doses of MO at 3 dpf using live automated imaging of the *-1.4col1a1:egfp* transgene (*45*). Consistent with our observations with the MAP4K4 inhibitor compound, we noted a dose-dependent exacerbation of CFA, as indicated by broadening of the ceratohyal angle and shortening of the mandible, while body length was decreased significantly only at the

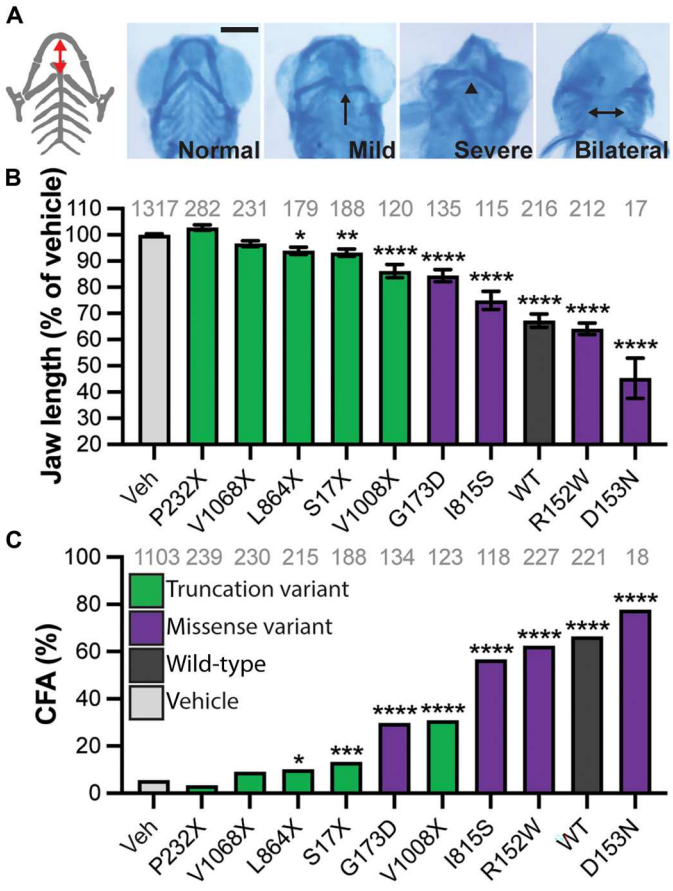

Fig. 4. Ectopic *MAP4K4* expression causes CFAs at 5 dpf. (**A**) Representative ventral view of Alcian blue staining of jaw cartilage. Schematic of the cartilages shown in gray with the distance between the Meckel's and ceratohyal cartilages shown by a red arrow. Malformations included misshapen cartilage (arrow), increased angle between ceratohyal cartilages (arrowhead), and bilateral positioning of cartilage (double-headed arrow). (**B**) Jaw length was measured and normalized to the average of the vehicle-injected siblings (Veh) and is reduced by expression of *MAP4K4*^{WT} and missense variants. (**C**) The incidence of malformations was quantified as a percentage of total larvae showing a defect. Scale bar, 200 μm (A). Graphs (B to C): pale gray, vehicle; dark gray, *MAP4K4*^{WT}; purple, missense variants; green, truncation variants. *P < 0.05; **P < 0.01; ***P < 0.001; ****P < 0.0001 by pairwise Student's t test (B) or chi-square test (C) compared to vehicle. ANOVA gives P < 0.0001 for (B). n numbers are inset to graphs in gray text. Error bars represent the SEM.

highest dose (Fig. 7, A to C; and fig. S1, D to H). Furthermore, we injected MO in *cmlc2:gfp* cardiac reporter (*46*) embryos and noted a significant increase in atrium and ventricle chamber size at maximum diastole at 2 dpf, a direct proxy for cardiac defects observed in human cases. Both the cardiac chamber size and jaw phenotypes were rescued significantly by coinjection of *MAP4K4*^{WT} mRNA (Fig. 7).

MAP4K4 is a negative regulator of RAS signaling in early zebrafish embryo

Loss of endogenous Map4k4 function affects similar tissues to those affected in affected individuals, supporting the model that loss of MAP4K4 function causes RASopathy-like disease. Accordingly, MAP4K4 acts as a negative regulator of RAS signaling in the early

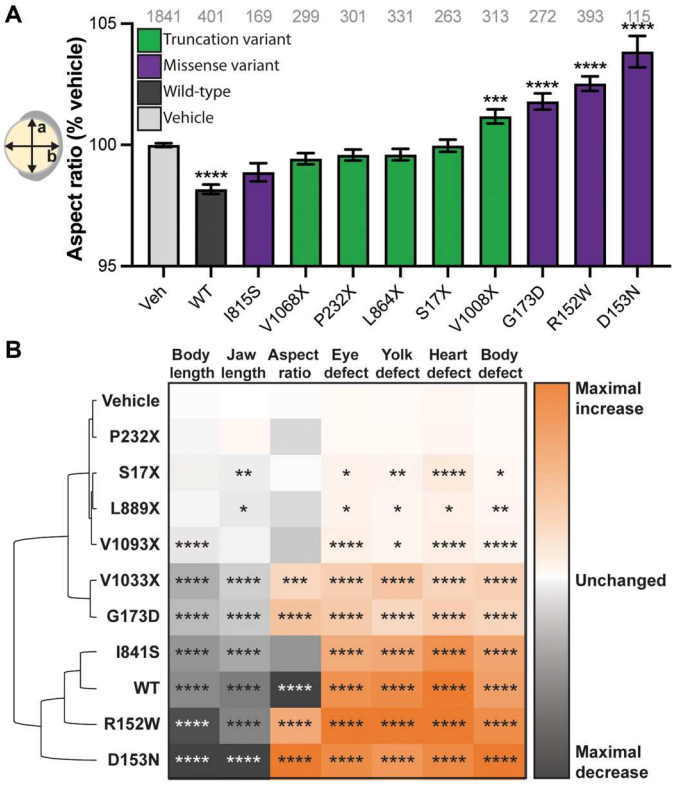

Fig. 5. Increasing and decreasing *MAP4K4* has similar effects on development. (**A**) Aspect ratio was measured at 11 hours post fertilization (hpf) as the ratio of a divided by b, shown on the embryo schematic. WT and hypomorphic variants reduce the aspect ratio, loss-of-function (LOF) variants have no effect, and dominant-negative (DN) variants elongate the embryo. (**B**) Hierarchical clustering of the quantitative phenotypic metrics ranks DN alleles as closer to *MAP4K4*^{WT} in phenotypic output than to loss of function alleles. The P value for each measurement is shown in the box, with the absence of symbols indicating nonsignificant changes. Graph: pale gray, vehicle; dark gray, *MAP4K4*^{WT}; purple, missense variants; green, truncation variants. *P < 0.05; **P < 0.01; ***P < 0.001; ****P < 0.0001 by pairwise Student's t test compared to vehicle. ANOVA gives P < 0.0001 for (A). n numbers are inset to graph in gray text. Error bars represent the SEM.

zebrafish embryo (Fig. 5A). To confirm this, we tested the ability of *MAP4K4*^{WT} to restrain hyperactive RAS signaling, which can be induced by ectopic expression of *MEK1*^{F53L} mRNA (*44*), a cancer-associated variant (Fig. 8A). Increased signaling then causes embryo elongation at 11 hpf. Coexpression of *MAP4K4*^{WT} rescues this morphological defect significantly, but by contrast, the LOF variant *MAP4K4*^{L889X} only partially ameliorates the aspect ratio elongation. Thus, increasing the levels of MAP4K4 in the embryo can counter the morphological effects of increasing RAS pathway activity, consistent with a role as a negative pathway regulator.

We also tested whether the embryo elongation observed upon expression of *MAP4K4*^{D153N} is caused by hyperactive RAS signaling. We treated injected embryos with either PD0325901, a MEK inhibitor, or SU5402, a fibroblast growth factor receptor (FGFR) inhibitor (Fig. 8B). Treatment with either drug reduced the aspect ratio of vehicle-injected embryos and those expressing *MAP4K4*^{D153N}.

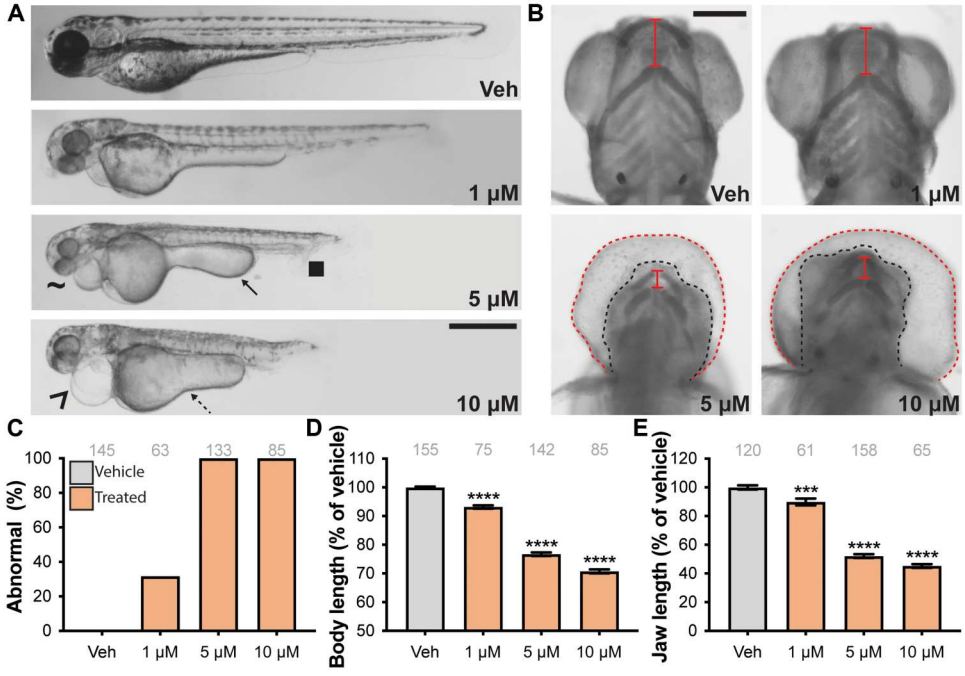

Fig. 6. Pharmacological inhibition of Map4k4 impacts similar tissues to those affected in affected individuals. (**A** and **B**) WT embryos were treated with different doses of the MAP4K4 inhibitor PF06260933. (A) At 3 dpf, Map4k4 inhibition induced developmental defects including shortening of the body, small eyes (~), cloacal defects (closed square), pericardial edema (^), and thickening of the yolk extension (arrow) or reduced yolk constriction (dashed arrow). Representative lateral images are shown. (B) Representative ventral images of Alcian blue staining of the jaw cartilage at 5 dpf. At higher doses, the swollen hearts obscure the jaw. For clarity, the black dashed line outlines the head, the red dashed line outlines edematous heart, and the solid red line indicates the distance between the ceratohyal and Meckel's cartilages. (**C** to **E**) Quantitation of abnormalities (C), body length (D), and jaw length (E) reveals increasing defects and shortening of both body and jaw in a dose-responsive manner. Scale bars, 500 (A) and 200 μm (B). Graphs: pale gray: vehicle (Veh); orange, drug treated. *$P < 0.05$; **$P < 0.01$; ***$P < 0.001$; ****$P < 0.0001$ by pairwise Student's *t* test (D and E) compared to vehicle. ANOVA gives $P < 0.0001$ for (D) and (E). *n* numbers are inset to graphs in gray text. Error bars represent the SEM.

Together, these data suggest that embryo elongation in the context of MAP4K4 ablation is mediated through elevated RAS signaling.

We further tested this hypothesis that MAP4K4 affects RAS signaling at the molecular level. Embryos were injected with MAP4K4WT, and protein was extracted at 50% epiboly, a time point at which we have previously shown that hyperactivation of the RAS pathway causes increased levels of dually phosphorylated ERK (dpERK) at the blastoderm margin. We performed Western blotting, quantified band intensity using ImageJ, and normalized the level of dpERK to the amount of total ERK (Fig. 8C).

Overexpression of MEKF53L, a variant of MEK associated with cancer and shown to increase RAS signaling, caused an increase in the amount of dpERK consistent with hyperactivation of the pathway. Conversely, overexpression of MAP4K4WT caused a statistically significant decrease in the amount of dpERK compared to uninjected siblings, suggesting that increasing MAP4K4 levels inhibits the RAS signaling pathway at the molecular level. This decrease is smaller than the extent of the change caused by overexpression of MEKF53L but is consistent with the fact that we observe a smaller effect on aspect ratio at 11 hpf for MAP4K4WT overexpression than observed for MEKF53L overexpression (Fig. 8B). This is likely due to the fact that MEKF53L is associated with cancer rather than RASopathies and cancer-associated mutations disrupt the pathway more severely. Thus, increasing the levels of MAP4K4 in the embryo can counter the morphological effects of increasing RAS pathway activity, consistent with a role as a negative pathway regulator.

DISCUSSION

Here, we report *MAP4K4* as the cause of a previously undescribed syndrome with phenotypes overlapping with RASopathy syndromes. These heterozygous pathogenic variants are reported here in 26 individuals from 21 pedigrees. Individuals display overlapping clinical features affecting development of the brain, heart, and face. Affected individuals with rare variants in *MAP4K4* should be clinically assessed, as they are at risk of DD, cardiac disease, renal disease, hearing loss, short stature, and neurobehavioral differences.

Functional studies in zebrafish showed that *MAP4K4* variants caused hypomorphic, LOF, or DN effects. The missense variants identified in our cohort were mostly clustered within the kinase domain (Fig. 1A). Arg^{152} and Asp^{153} are both found within the arginine-glycine-aspartic acid (RGD) motif of the catalytic loop, while Gly^{173} is located within the activation loop, close to the adenosine 5′-triphosphate (ATP) binding region. The variants at these residues all acted as DN alleles, consistent with a reduction in kinase activity with no effect on protein interaction.

It is expected that the truncation variants would abolish protein function, but previous studies into the role of the CNH domain have been contradictory (*10*, *11*). In our studies, truncating MAP4K4 at p.Ser17, p.Pro232, p.Leu864, or p.Val1068 all caused loss of protein

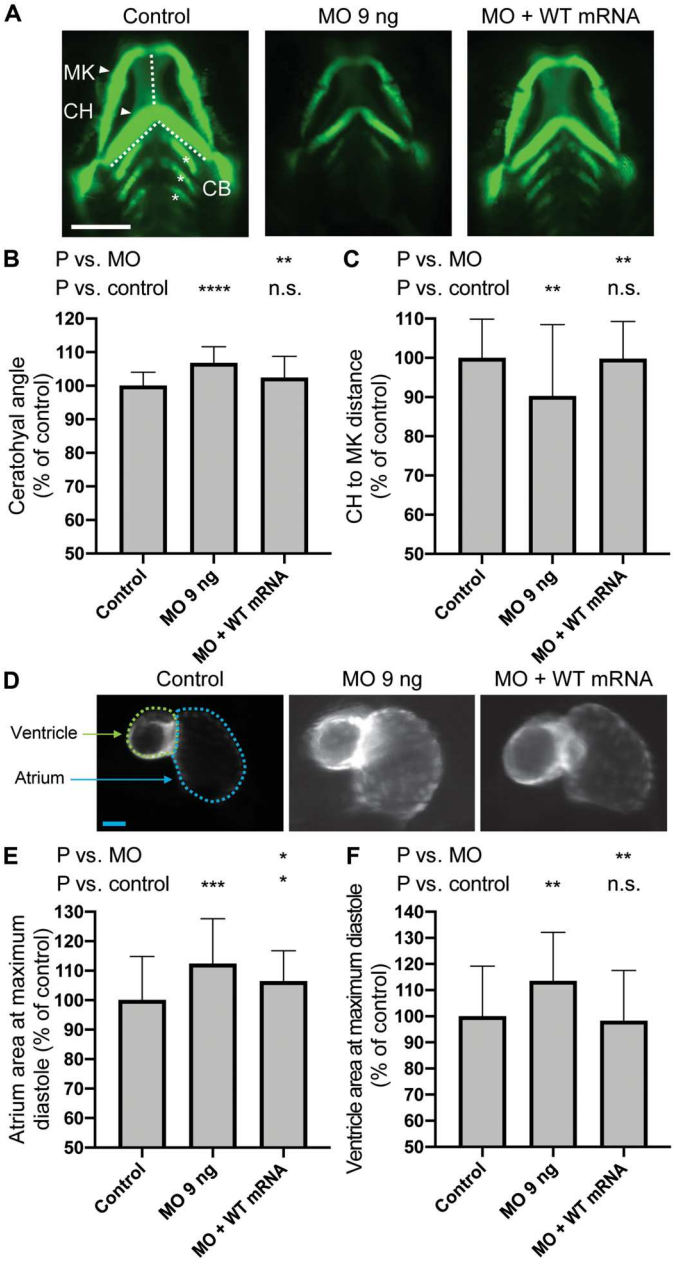

Fig. 7. *map4k4* ablation results in altered craniofacial patterning and cardiac phenotypes in zebrafish larvae. (**A**) Representative ventral images show cartilage structures in the anterior region of *-1.4col1a1:egfp* zebrafish larvae at 3 dpf for control, morpholino (MO), and MO rescued with WT human *MAP4K4* mRNA. Adjoining white dashed lines indicate the ceratohyal (CH) angle; vertical dashed line indicates the distance from Meckel's cartilage (MK) to CH. CB, ceratobranchial arches. (**B** and **C**) Quantification of CH angle and CH to MK distance measurements on ventral green fluorescent protein–positive (GFP^+) images acquired at 3 dpf [as shown in (A)]; n = 35 to 40 larvae per batch, repeated. (**D**) Representative ventral images of cardiac chambers of *cmlc2:egfp* zebrafish larvae at 2 dpf. (**E** and **F**) Quantification of atrium and ventricle area measured on ventral images at maximum diastole [as shown in (D)]; n = 38 to 45 larvae per batch, repeated. For (B), (C), (E), and (F), each condition is normalized to its respective experimental control and expressed as a percentage. Scale bars, 300 (A) and 200 μm (D). *P < 0.05; **P < 0.01; ***P < 0.001; ****P < 0.0001; n.s., not significant, by pairwise Student's t test compared to vehicle. Error bars represent the SEM.

function. p.Val1093Ter contains the sequence for the full kinase domain and interdomain, and half of the CNH domain, while p.Ser17Ter contains no functional domains. This may indicate either that the truncated protein does not fold, no matter its length, or that the complete CNH domain is necessary for protein function.

A subset of identified variants disrupts the canonical splice site sequences (Fig. 1B), but specimens were unavailable for experimental testing of mRNA splicing. A splice acceptor site is disrupted by c.695-3del, and we predict that this will cause skipping of the subsequent exon. Loss of exon 9 would be predicted to cause a frameshift (p.Pro232ArgfsTer8), which we modeled using the p.Pro232Ter variant and showed to be a LOF variant. A splice donor site is disrupted by c.639+1G>C, and we predict that this variant will cause skipping of the preceding exon, exon 7, during splicing. Loss of exon 7 would be predicted to cause a frameshift of the protein (p.Leu169fsTer2), which would likely be a LOF allele.

By extrapolating from our functional data for a subset of variants, we can make predictions about the allelic series (Table 2). We cannot exclude the possibility of nonsense-mediated decay causing loss of the mRNA before translation in patients, such that the protein would never be expressed regardless of the predicted variant. Furthermore, we engineered the truncation variants to introduce stop codons instead of frameshifts. It is therefore possible that frameshift variants act slightly differently in patients than in our overexpression assays. However, our data suggest that all variants reduce protein function, even if they do so by reducing the amount of mRNA expressed.

MAP4K4 was previously shown to be required for embryonic development. In *Drosophila*, the MAP4K4 homolog misshapen is required for dorsal closure during embryogenesis (*14*). MO-mediated knockdown in zebrafish was reported to cause mild gastrulation defects, but these were not characterized (*15*). Complete loss of *Map4k4* is embryonic lethal in mice, causing posterior truncation, while endothelial cell–specific deletion causes vascular defects and early postnatal lethality (*13*, *16*). Deleting *Map4k4* from adult mice, however, had little effect on tissue homeostasis (*47*).

The precise function of MAP4K4 in regulating the RAS pathway remains unclear. MAP4K4 was shown to associate with FGFR1, an RTK that signals via RAS, and to be required for mediating an FGF-induced signal (*31*). Furthermore, MAP4K4 can inhibit protein phosphatase 2A (PP2A), which itself can dephosphorylate ERK to inactivate signaling (*30*). Treating $MAP4K4^{D153N}$-injected embryos with a MEK inhibitor prevents elongation of the embryonic axis, suggesting that MAP4K4 may inhibit RAS signaling upstream of MEK. This would exclude the possibility of MAP4K4 modulating the pathway via PP2A, which exerts its effects on ERK (*30*). Accordingly, the actions of MAP4K4 upon PP2A were reported to positively regulate the pathway, while we found that MAP4K4 was an inhibitor of signaling.

MAP4K4 has also been reported to be necessary to inhibit RAS signaling and maintain endothelial cell fate, potentially by activating Ras p21 protein activator 1 (RASA1), a guanosine triphosphatase (GTPase)–activating protein that promotes inactivation of RAS (*13*). Because RASA1 is upstream of MEK and inhibits signaling by enhancing the GTPase activity of RAS, it represents a plausible candidate for affecting the role of MAP4K4 in the pathway. RASA1 was shown to interact with MAP4K4 to maintain endothelial fate in mouse by inhibiting signaling, although it has roles beyond

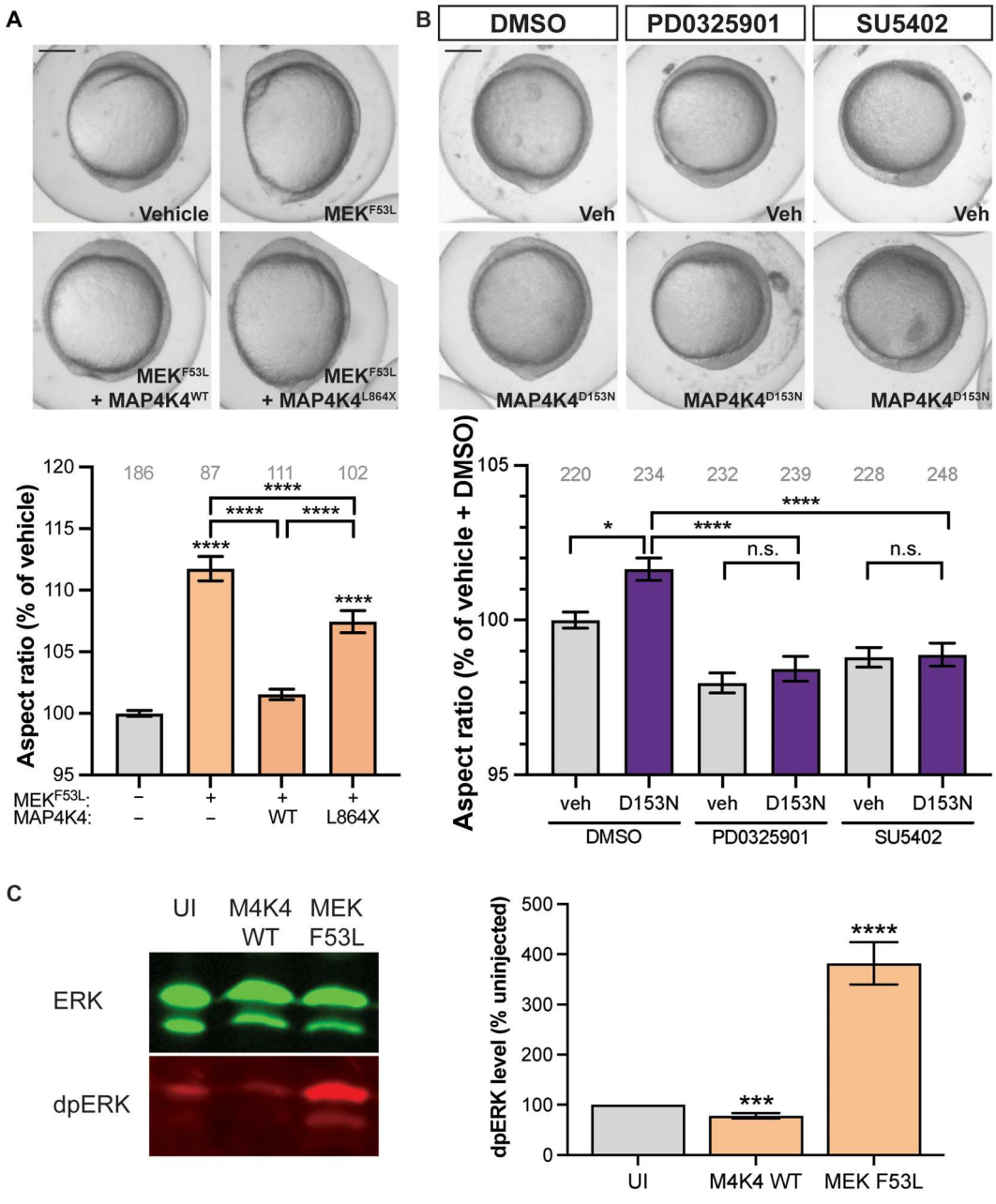

Fig. 8. MAP4K4 is a negative regulator of RAS signaling. (**A**) Embryos were injected with a hyperactive variant of *MEK*, *MEK*^{F53L}, in combination with *MAP4K4* variants. Embryos were imaged at 11 hpf, and the aspect ratio was calculated. *MEK*^{F53L} increases aspect ratio, and this elongation is rescued by *MAP4K4*^{WT} but not *MAP4K4*^{L889X}. (**B**) Embryos were injected with *MAP4K4*^{D153N} and then treated with an inhibitor of MAPK kinase (MEK), PD0325901, or the fibroblast growth factor receptor (FGFR), SU5402. Embryos were imaged at 11 hpf, and the aspect ratio was calculated. Inhibiting ligand binding or MEK activity rescues the elongation caused by *MAP4K4*^{D153N}. DMSO, dimethyl sulfoxide. (**C**) Western blotting with quantification and normalization of the level of dually phosphorylated extracellular signal–regulated kinase (dpERK) to the amount of total ERK. Scale bars, 250 μm (A and B). Graph (A): pale gray, vehicle (Veh); orange, drug treated. Graph (B): pale gray, vehicle; purple, *MAP4K4*^{D153N}. *$P < 0.05$; **$P < 0.01$; ***$P < 0.001$; ****$P < 0.0001$ by pairwise Student's *t* test compared to vehicle. ANOVA gives $P < 0.0001$ for (A) and (B). *n* numbers are inset to graphs in gray text. Error bars represent the SEM.

angiogenesis (*13*). Furthermore, RASA1 is involved in the pathogenesis of diverse conditions, including CHD and cancer (*48*), while MAP4K4 has also been implicated in cancer (*12*, *17*, *20*, *25*, *26*), and we link it to CHD in our work. Thus, the effects of MAP4K4 on RAS signaling may be mediated through RASA1, although it is possible that additional targets are involved. MAP4K4 is also known to act through c-Jun N-terminal signaling, which would be of interest to test in further experiments.

MAP4K4 is likely haplosensitive. This is consistent with our finding that the levels of MAP4K4 must be maintained within a window of activity to promote proper embryonic development. This conclusion may be explained by the fact that variants that

Table 2. Predicted impact of *MAP4K4* variants upon protein function. DN, dominant negative; LOF, loss of function; CNH, citron homology; ATP, adenosine 5′-triphosphate.

Variant	Location	Predicted impact on gene and protein	Allele type
c.46-47dup p.Ser17ProfsTer55	N terminus	Frameshift: loss of kinase domain, interdomain, and CNH	LOF demonstrated
c.52delC p.Leu18CysfsTer53	N terminus	Frameshift: loss of kinase domain, interdomain, and CNH	LOF predicted
c.116 T>G p.Val39Gly	P loop, kinase domain	Loss of kinase activity: Val^{39} is criptical for ATP binding within the P loop	DN predicted
c.328G>A p.Ala110Thr	Kinase domain	Loss of kinase activity: not a known critical residue but lies close to ATP binding site and likely reduce kinase function	DN predicted
c.391G>A p.Ala131Thr	Kinase domain	Loss of kinase activity: not a known critical residue but lies close to ATP binding site and likely reduce kinase function	DN predicted
c.454C>T p.Arg152Trp	RGD motif, kinase domain	Loss of kinase activity: Arg^{152} is part of the RGD motif of the catalytic loop	DN demonstrated
c.639+1G>C p.Leu169fsTer2	Splice donor site	Excision of exon 7 from the transcript. Frameshift: truncation of kinase domain, loss of interdomain and CNH	LOF predicted
c.518G>A p.Gly173Asp	Activation loop, kinase domain	Loss of kinase activity: Gly^{173} is the activation loop, close to the ATP binding region	DN demonstrated
c.560C>G p.Thr187Arg	Activation loop, kinase domain	Loss of kinase activity: Thr^{187} lies in the activation loop	LOF predicted
c.695-3delC p.Pro232LfsTer8	Splice acceptor site	Excision of exon 9 from transcript. Frameshift: truncation of the kinase domain, loss interdomain and CNH	LOF demonstrated
c.736C>T p.Pro246Ser	Kinase domain	Loss of kinase activity: Pro^{246} is not a known critical residue, but variants likely reduce kinase function	DN predicted
c.1489C>T p.Arg497Ter	Interdomain	Premature stop codon: truncation of the interdomain and loss of CNH	LOF predicted
c.2426T>G p.Ile836Ser	Interdomain	Reduced function or disrupted regulation: The interdomain harbors protein interaction sites and phosphorylation sites	LOF predicted
c.2591T>A p.Leu864Ter	Interdomain	Premature stop codon: truncation of the interdomain, loss of CNH	LOF demonstrated
c.3023-42del p. Val1008GlyfsTer19	CNH domain	Frameshift: truncation of CNH. DN properties may suggest possible autoinhibitory region within CNH	DN demonstrated
c.3146C>T p.Ala1049Val	CNH domain	Reduced function: CNH domain regulates kinase function and contains protein interaction sites that may be disrupted	LOF predicted
c.3197-3200dup p.Val1068IlefsTer4	CNH domain	Frameshift: truncation of the CNH	LOF demonstrated
c.3218-9del p. Tyr1147TrpfsTer61	CNH domain	Frameshift: truncation of the CNH	LOF predicted
c.3469C>T p.Gln1157Ter	CNH domain	Premature stop codon: truncation of the CNH	LOF predicted

increase RAS signaling can ultimately lead to reduced pathway activity (*42*). Considering the similarity of the phenotypic consequences of increasing and decreasing MAP4K4 function, it is possible that many of the developmental defects observed here are caused by down-regulation of signaling. If that is the case, then increasing WT MAP4K4 levels would cause inhibition of signaling, while reducing protein function by supplying DN MAP4K4 would initially lead to activation of the pathway, followed by down-regulation in response to negative feedback. The fact that elevated amounts of MAP4K4 are detected in conditions such as cancer, atherosclerosis, and diabetes and that reducing MAP4K4 activity can rescue the disease state lends further support to the critical importance of maintaining MAP4K4 at a suitable level (*12*, *19*, *23*, *26*–*28*).

In summary, we have added *MAP4K4* to the repertoire of genes that may be associated with RASopathy-like developmental disease. Targeted reduction of MAP4K4 activity has been touted as a possible therapeutic approach for diverse conditions (*23*, *27*), yet we

demonstrate that abrogation of MAP4K4 function is also associated with disease. The implications of our work, therefore, suggest that care must be taken not to reduce activity too far at the risk of exacerbating disease. Despite this caveat, MAP4K4 remains an attractive target for pharmacological modulation of RAS signaling in humans.

MATERIALS AND METHODS

This study was approved by the Institutional Review Board (IRB) of the Children's Hospital of Philadelphia. Informed consent was obtained from all individual participants included in the study. Additional informed consent was obtained from all individual participants for whom identifying information is included here.

Exome and genome sequencing

Genomic DNA was extracted from whole blood from the affected children and their parents. The original patients were enrolled under an approved IRB from the Children's Hospital of Philadelphia. Exome or genome sequencing was performed with a variety of standard capture kits and the general assertion criteria for variant classification following American College of Medical Genetics and Genomics, Association of Molecular Pathology (ACMGG/AMP) guidelines (*49*). There were no other variants in these patients who survived filtration and analysis using either dominant or recessive models and could explain the phenotypes.

Zebrafish strains and husbandry

Zebrafish were maintained, and all experiments conducted according to Princeton University or Northwestern University Institutional Animal Care and Use Committee–approved protocols. The PWT strain (*50*) was used for injection of mRNA; *-1.4col1a1:gfp* (*45*) and *cmlc2:gfp* (*46*) transgenic lines were used for *map4k4* knockdown studies. Embryos were raised at 28°C until phenotypic end point.

Pharmacological treatment of zebrafish embryos

PF06260933 (Sigma-Aldrich) was added immediately following embryo collection to a final concentration of 1, 5, or 10 μM. Water was changed on the second day, with fresh drug applied. For inhibition of MEK, PD0325901 (Sigma-Aldrich) in dimethyl sulfoxide (DMSO) was added to a final concentration of 1 μM, while the FGFR inhibitor SU5402 (Sigma-Aldrich) in DMSO was used at a concentration of 5 μM. These concentrations were previously shown to rescue embryo elongation caused by MEK (*43*, *44*). Control embryos were treated with an equivalent amount of DMSO. Both drugs were applied from 4.5 hpf until imaging (*35*).

Cloning and site-directed mutagenesis

pDONR223-MAP4K4 was a gift from W. Hahn and D. Root (Addgene, plasmid no. 23486) (*34*). This construct contains human *MAP4K4* transcript variant 13 (NM_001384485.1) with a deletion of six nucleotides (Δ2078–2083). The human MAP4K4 sequence was subcloned into pCS2+ and tagged with mCherry and a p2A termination sequence. Plasmids were transfected into 5-alpha competent cells (New England Biolabs) and purified using the QIAprep Spin Miniprep Kit (QIAGEN) or the Quantum Prep Plasmid Midiprep Kit (Bio-Rad). Overlapping primers (Integrated DNA Technologies) were designed to contain base changes corresponding to variants identified in affected individuals, obtained from Integrated DNA Technologies, and used in a PCR to introduce changes to the plasmid sequence. Sequence changes were verified by Sanger sequencing (GeneWiz).

mRNA transcription and microinjection in zebrafish

mRNA was generated using the mMESSAGE mMACHINE Sp6 kit (Invitrogen) according to the manufacturer's instructions and quantified using a NanoDrop One (Thermo Fisher Scientific). Embryos were injected as described (*51*) using a PV820 Pneumatic PicoPump (World Precision Instruments). Embryos at the one- to four-cell stages were injected with 150 pg of MAP4K4 mRNA and/or 55 pg of MEK mRNA suspended in 500 pl of phenol red (phenolsulfonphthalein; 5 mg/ml)/0.2 M KCl. Vehicle-injected embryos received 500 pl of phenol red (5 mg/ml)/0.2 M KCl. For each variant, at least three clutches of at least 30 embryos each were injected, with mRNA generated on at least two separate occasions.

Transient suppression of *map4k4* in zebrafish

A splice-blocking MO was designed to target the exon 13 splice donor site of *Danio rerio map4k4* (ENSDART00000165230.2; e13i13; Gene Tools). We injected 1 nl of MO at different doses (3, 6, and 9 ng) into one- to four-cell–staged zebrafish embryos. MO efficiency was validated by extracting total RNA from pools of 2 dpf embryos (30 animals per condition; controls and MO injected) using TRIzol (Thermo Fisher Scientific) according to the manufacturer's instructions. cDNA was synthesized with the QuantiTect RT kit (QIAGEN). We performed RT-PCR of the MO target using flanking primers, and resulting PCR product was migrated on a 1% agarose gel. Bands were excised, and PCR product was purified with the QIAquick Gel Extraction Kit (QIAGEN) and cloned in TOPO-TA vector (Thermo Fisher Scientific). Purified plasmid from resulting colonies (n = 4 per PCR product) were sequenced using BigDye 3.1 terminator chemistry according to standard protocols. Rescue experiments were carried out with 9 ng of *map4k4* MO and 150 pg of WT human *MAP4K4* mRNA.

Alcian blue staining for zebrafish craniofacial analysis

Larvae were euthanized at 5 dpf and fixed in 4% paraformaldehyde/phosphate-buffered saline (PBS) overnight. Larvae were washed in PBS, dehydrated through an ethanol series to 70% EtOH, and incubated in 0.04% Alcian blue 8GX/50 mM $MgCl_2$/70% EtOH overnight at 4°C. After several rinses in 70% EtOH, embryos were rehydrated through an ethanol series to 0.1% Tween 20/PBS, washed in 2% KOH, bleached in 1% H_2O_2/2% KOH, washed in 2% KOH, and then processed through a glycerol series to 80% glycerol/2% KOH for imaging.

Zebrafish imaging and analysis

mRNA-injected embryos were imaged using a Leica M205 FA stereoscope with a DFC365FX or DFC450C camera attachment. For imaging at 3 dpf, embryos were immobilized in tricaine (ethyl-3-aminobenzoate methane sulfonate salt; 0.08 mg/ml; Sigma-Aldrich), which was removed after image acquisition. Phenotypic abnormalities were manually scored for each embryo, and prevalence was calculated as a percentage of all embryos injected with that condition.

MO-injected larvae were tricaine-anesthetized at 3 dpf, and craniofacial features were imaged using the Vertebrate Automated Screening Technology (VAST) BioImager (Union Biometrica) mounted to an Axio Imager.M2m microscope (Zeiss) with a 10×

objective lens. Larvae were passed sequentially through a 600-mm capillary on the detection platform. Each larva was detected and oriented automatically for ventral [green fluorescent protein (GFP)] or lateral (brightfield) images with a preprovided template setting in the VAST software (version 1.2.6.7) operated in automatic imaging mode with a 70% minimum similarity threshold, as described (*52*). We captured fluorescent images from ventrally positioned larvae with an Axiocam 503 monochrome camera (Zeiss) and ZenPro software (Zeiss). For heart phenotyping, we captured GFP signal of the ventral aspect of live embryos with a Nikon AZ100 microscope facilitated by a Nikon camera controlled by Nikon NIS-Elements Software at 2 dpf. For aspect ratio phenotyping of gastrulating embryos, we captured brightfield images at 11 hpf with a Nikon SMZ745 stereoscope and Nikon digital sight camera.

ImageJ was used to measure the lengths of the major and minor axes of the yolk at 11 hpf, the length of the embryo at 3 dpf, the ceratohyal angle and the distance between the ceratohyal and Meckel's cartilages at 3 and 5 dpf, and the area of heart chambers at 2 dpf. Measurements were performed with the investigator masked to experimental condition and normalized to the mean of the vehicle-injected control group to allow combination of embryos from multiple clutches. A one-way analysis of variance (ANOVA) with Bonferroni correction was performed to compare the whole group, while pairwise Student's *t* tests were used to compare variant-injected embryos to vehicle-injected controls. Hierarchical clustering was performed using RStudio.

Protein extraction and Western blotting

A total of 100 injected embryos were incubated in pronase (1.3 mg/ml; Sigma-Aldrich) at 28°C for 5 min, and then chorions were removed by agitation at 50% epiboly. Embryos were rinsed three times in E3 buffer (5 mM NaCl, 0.17 mM KCl, 0.33 mM $CaCl_2$, and 0.33 mM $MgSO_4$), then resuspended in 200 μl of E3 buffer, and homogenized by pipetting. One milliliter of 0.5× Ringer's solution (50 mM NaCl, 10 mM KCl, and 1.25 μM $NaHCO_3$) was added, and samples were vortexed before cells were precipitated by centrifugation [300 relative centrifugal force (rcf), 1 min, 4°C]. Cells were resuspended in 50 μl of lysis buffer [20 mM tris (pH 8.0), 50 mM NaCl, 2 mM EDTA, 1% Igepal CA-630, and 200 μM phenylmethylsulfonyl fluoride] with protease inhibitor cocktail (Sigma-Aldrich), and debris was pelleted (14,000 rcf, 10 min, 4°C). Equal amounts of protein lysate were prepared by adding NuPAGE LDS sample buffer and reducing agent (Thermo Fisher Scientific) and boiling at 100°C for 10 min. SDS–polyacrylamide gel electrophoresis was performed using 4 to 12% Tris-Bis NuPAGE gels and the XCell SureLock Mini-Cell Electrophoresis system (Thermo Fisher Scientific) according to the manufacturer's instructions. Proteins were transferred to nitrocellulose (Li-COR) and blocked with 5% milk powder in 1% Tween 20/PBS (PBT), and primary antibody (Cell Signaling Technology) was applied at 1:1000 dilution in 5% bovine serum albumin (BSA; Sigma-Aldrich)/PBT. Membranes were incubated with shaking overnight at 4°C and then washed with PBT. Fluorescently labeled secondary antibody (Li-COR, Invitrogen) was applied at 1:5000 dilution in 5% BSA/PBT, and membranes were incubated with shaking for 1 hour at room temperature and then washed with PBT. Membranes were imaged using the Azure 600 imager, and band intensity was quantified using ImageJ.

Supplementary Materials

This PDF file includes:
Legend for table S1

Other Supplementary Material for this manuscript includes the following:
Table S1

View/request a protocol for this paper from *Bio-protocol*.

REFERENCES AND NOTES

1. D. K. Simanshu, D. V. Nissley, F. McCormick, RAS proteins and their regulators in human disease. *Cell* **170**, 17–33 (2017).
2. C. X. Deng, A. Wynshaw-Boris, M. M. Shen, C. Daugherty, D. M. Ornitz, P. Leder, Murine FGFR-1 is required for early postimplantation growth and axial organization. *Genes Dev.* **8**, 3045–3057 (1994).
3. T. P. Yamaguchi, K. Harpal, M. Henkemeyer, J. Rossant, fgfr-1 is required for embryonic growth and mesodermal patterning during mouse gastrulation. *Genes Dev.* **8**, 3032–3044 (1994).
4. W. E. Tidyman, K. A. Rauen, The RASopathies: Developmental syndromes of Ras/MAPK pathway dysregulation. *Curr. Opin. Genet. Dev.* **19**, 230–236 (2009).
5. K. A. Rauen, The RASopathies. *Annu. Rev. Genomics Hum. Genet.* **14**, 355–369 (2013).
6. G. A. Jindal, Y. Goyal, R. D. Burdine, K. A. Rauen, S. Y. Shvartsman, RASopathies: Unraveling mechanisms with animal models. *Dis. Model. Mech.* **8**, 769–782 (2015).
7. A. R. Grant, B. J. Cushman, H. Cavé, M. W. Dillon, B. D. Gelb, K. W. Gripp, J. A. Lee, H. Mason-Suares, K. A. Rauen, M. Tartaglia, L. M. Vincent, M. Zenker, Assessing the gene-disease association of 19 genes with the RASopathies using the ClinGen gene curation framework. *Hum Mutat* **39**, 1485–1493 (2018).
8. Z. Yao, G. Zhou, X. S. Wang, A. Brown, K. Diener, H. Gan, T. H. Tan, A novel human STE20-related protein kinase, HGK, that specifically activates the c-Jun N-terminal kinase signaling pathway. *J. Biol. Chem.* **274**, 2118–2125 (1999).
9. E. Delpire, The mammalian family of sterile 20p-like protein kinases. *Pflugers Arch.* **458**, 953–967 (2009).
10. Y. C. Su, J. Han, S. Xu, M. Cobb, E. Y. Skolnik, NIK is a new Ste20-related kinase that binds NCK and MEKK1 and activates the SAPK/JNK cascade via a conserved regulatory domain. *EMBO J.* **16**, 1279–1290 (1997).
11. S. Kaneko, X. Chen, P. Lu, X. Yao, T. G. Wright, M. Rajurkar, K. I. Kariya, J. Mao, Y. T. Ip, L. Xu, Smad inhibition by the Ste20 kinase Misshapen. *Proc. Natl. Acad. Sci. U.S.A.* **108**, 11127–11132 (2011).
12. J. H. Wright, X. Wang, G. Manning, B. J. LaMere, P. le, S. Zhu, D. Khatry, P. M. Flanagan, S. D. Buckley, D. B. Whyte, A. R. Howlett, J. R. Bischoff, K. E. Lipson, B. Jallal, The STE20 kinase HGK is broadly expressed in human tumor cells and can modulate cellular transformation, invasion, and adhesion. *Mol. Cell Biol.* **23**, 2068–2082 (2003).
13. R. J. Roth Flach, C. A. Guo, L. V. Danai, J. C. Yawe, S. Gujja, Y. J. K. Edwards, M. P. Czech, Endothelial mitogen-activated protein kinase kinase kinase kinase 4 is critical for lymphatic vascular development and function. *Mol. Cell Biol.* **36**, 1740–1749 (2016).
14. S. Noselli, JNK signaling and morphogenesis in *Drosophila*. *Trends Genet.* **14**, 33–38 (1998).
15. M. Koppen, B. G. Fernandez, L. Carvalho, A. Jacinto, C. P. Heisenberg, Coordinated cell-shape changes control epithelial movement in zebrafish and *Drosophila*. *Development* **133**, 2671–2681 (2006).
16. Y. Xue, X. Wang, Z. Li, N. Gotoh, D. Chapman, E. Y. Skolnik, Mesodermal patterning defect in mice lacking the Ste20 NCK interacting kinase (NIK). *Development* **128**, 1559–1572 (2001).
17. C. S. Collins, J. Hong, L. Sapinoso, Y. Zhou, Z. Liu, K. Micklash, P. G. Schultz, G. M. Hampton, A small interfering RNA screen for modulators of tumor cell motility identifies MAP4K4 as a promigratory kinase. *Proc. Natl. Acad. Sci. U.S.A.* **103**, 3775–3780 (2006).
18. X. Tang, A. Guilherme, A. Chakladar, A. M. Powelka, S. Konda, J. V. Virbasius, S. M. C. Nicoloro, J. Straubhaar, M. P. Czech, An RNA interference-based screen identifies MAP4K4/NIK as a negative regulator of PPARgamma, adipogenesis, and insulin-responsive hexose transport. *Proc. Natl. Acad. Sci. U.S.A.* **103**, 2087–2092 (2006).
19. K. Bouzakri, J. R. Zierath, MAP4K4 gene silencing in human skeletal muscle prevents tumor necrosis factor-alpha-induced insulin resistance. *J. Biol. Chem.* **282**, 7783–7789 (2007).
20. A. W. Liu, J. Cai, X. L. Zhao, T. H. Jiang, T. F. He, H. Q. Fu, M. H. Zhu, S. H. Zhang, ShRNA-targeted MAP4K4 inhibits hepatocellular carcinoma growth. *Clin. Cancer Res.* **17**, 710–720 (2011).
21. X. Zhao, R. Mohan, S. Ozcan, X. Tang, MicroRNA-30d induces insulin transcription factor MafA and insulin production by targeting mitogen-activated protein 4 kinase 4 (MAP4K4) in pancreatic β cells. *J. Biol. Chem.* **287**, 31155–31164 (2012).

22. W. J. Pannekoek, J. R. Linnemann, P. M. Brouwer, J. L. Bos, H. Rehmann, Rap1 and Rap2 antagonistically control endothelial barrier resistance. *PLOS ONE* **8**, e57903 (2013).
23. L. V. Danai, R. J. Roth Flach, J. V. Virbasius, L. Garcia Menendez, D. Y. Jung, J. H. Kim, J. K. Kim, M. P. Czech, Inducible deletion of protein kinase Map4k4 in obese mice improves insulin sensitivity in liver and adipose tissues. *Mol. Cell Biol.* **35**, 2356–2365 (2015).
24. R. J. Roth Flach, A. Skoura, A. Matevossian, L. V. Danai, W. Zheng, C. Cortes, S. K. Bhattacharya, M. Aouadi, N. Hagan, J. C. Yawe, P. Vangala, L. G. Menendez, M. P. Cooper, T. P. Fitzgibbons, L. Buckbinder, M. P. Czech, Endothelial protein kinase MAP4K4 promotes vascular inflammation and atherosclerosis. *Nat. Commun.* **6**, 8995 (2015).
25. K. Santhana Kumar, D. Tripolitsioti, M. Ma, J. Grählert, K. B. Egli, G. Fiaschetti, T. Shalaby, M. A. Grotzer, M. Baumgartner, The Ser/Thr kinase MAP4K4 drives c-Met-induced motility and invasiveness in a cell-based model of SHH medulloblastoma. *Springerplus* **4**, 19 (2015).
26. D. Tripolitsioti, K. S. Kumar, A. Neve, J. Migliavacca, C. Capdeville, E. J. Rushing, M. Ma, N. Kijima, A. Sharma, M. Pruschy, S. McComb, M. D. Taylor, M. A. Grotzer, M. Baumgartner, MAP4K4 controlled integrin β1 activation and c-Met endocytosis are associated with invasive behavior of medulloblastoma cells. *Oncotarget* **9**, 23220–23236 (2018).
27. M. E. Watts, C. Wu, L. L. Rubin, Suppression of MAP4K4 signaling ameliorates motor neuron degeneration in amyotrophic lateral sclerosis-molecular studies toward new therapeutics. *J. Exp. Neurosci.* **13**, 1179069519862798 (2019).
28. C. Wu, M. E. Watts, L. L. Rubin, MAP4K4 activation mediates motor neuron degeneration in amyotrophic lateral sclerosis. *Cell Rep.* **26**, 1143–1156.e5 (2019).
29. J. V. Virbasius, M. P. Czech, Map4k4 signaling nodes in metabolic and cardiovascular diseases. *Trends Endocrinol. Metab.* **27**, 484–492 (2016).
30. X. Gao, G. Chen, C. Gao, D. H. Zhang, S. F. Kuan, L. P. Stabile, G. Liu, J. Hu, MAP4K4 is a novel MAPK/ERK pathway regulator required for lung adenocarcinoma maintenance. *Mol. Oncol.* **11**, 628–639 (2017).
31. J. Li, S. Shi, S. P. Srivastava, M. Kitada, T. Nagai, K. Nitta, M. Kohno, K. Kanasaki, D. Koya, FGFR1 is critical for the anti-endothelial mesenchymal transition effect of N-acetyl-seryl-aspartyl-lysyl-proline via induction of the MAP4K4 pathway. *Cell Death Dis.* **8**, e2965 (2017).
32. N. L. Vora, B. Powell, A. Brandt, N. Strande, E. Hardisty, K. Gilmore, A. K. M. Foreman, K. Wilhelmsen, C. Bizon, J. Reilly, P. Owen, C. M. Powell, D. Skinner, C. Rini, A. D. Lyerly, K. A. Boggess, K. Weck, J. S. Berg, J. P. Evans, Prenatal exome sequencing in anomalous fetuses: New opportunities and challenges. *Genet. Med.* **19**, 1207–1216 (2017).
33. N. Sobreira, F. Schiettecatte, D. Valle, A. Hamosh, GeneMatcher: A matching tool for connecting investigators with an interest in the same gene. *Hum. Mutat.* **36**, 928–930 (2015).
34. C. M. Johannessen, J. S. Boehm, S. Y. Kim, S. R. Thomas, L. Wardwell, L. A. Johnson, C. M. Emery, N. Stransky, A. P. Cogdill, J. Barretina, G. Caponigro, H. Hieronymus, R. R. Murray, K. Salehi-Ashtiani, D. E. Hill, M. Vidal, J. J. Zhao, X. Yang, O. Alkan, S. Kim, J. L. Harris, C. J. Wilson, V. E. Myer, P. M. Finan, D. E. Root, T. M. Roberts, T. Golub, K. T. Flaherty, R. Dummer, B. L. Weber, W. R. Sellers, R. Schlegel, J. A. Wargo, W. C. Hahn, L. A. Garraway, COT drives resistance to RAF inhibition through MAP kinase pathway reactivation. *Nature* **468**, 968–972 (2010).
35. C. Anastasaki, A. L. Estep, R. Marais, K. A. Rauen, E. E. Patton, Kinase-activating and kinase-impaired cardio-facio-cutaneous syndrome alleles have activity during zebrafish development and are sensitive to small molecule inhibitors. *Hum. Mol. Genet.* **18**, 2543–2554 (2009).
36. C. Santoriello, G. Deflorian, F. Pezzimenti, K. Kawakami, L. Lanfrancone, F. d'Adda di Fagagna, M. Mione, Expression of H-RASV12 in a zebrafish model of Costello syndrome causes cellular senescence in adult proliferating cells. *Dis. Model. Mech.* **2**, 56–67 (2009).
37. R. A. Stewart, T. Sanda, H. R. Widlund, S. Zhu, K. D. Swanson, A. D. Hurley, M. Bentires-Alj, D. E. Fisher, M. I. Kontaridis, A. T. Look, B. G. Neel, Phosphatase-dependent and -independent functions of Shp2 in neural crest cells underlie LEOPARD syndrome pathogenesis. *Dev. Cell* **18**, 750–762 (2010).
38. V. Runtuwene, M. van Eekelen, J. Overvoorde, H. Rehmann, H. G. Yntema, W. M. Nillesen, A. van Haeringen, I. van der Burgt, B. Burgering, J. Hertog, Noonan syndrome gain-of-function mutations in NRAS cause zebrafish gastrulation defects. *Dis. Model. Mech.* **4**, 393–399 (2011).
39. C. Anastasaki, K. A. Rauen, E. E. Patton, Continual low-level MEK inhibition ameliorates cardio-facio-cutaneous phenotypes in zebrafish. *Dis. Model. Mech.* **5**, 546–552 (2012).
40. M. A. Razzaque, Y. Komoike, T. Nishizawa, K. Inai, M. Furutani, T. Higashinakagawa, R. Matsuoka, Characterization of a novel KRAS mutation identified in Noonan syndrome. *Am. J. Med. Genet. A* **158A**, 524–532 (2012).
41. M. Bonetti, J. Paardekooper Overman, F. Tessadori, E. Noël, J. Bakkers, J. den Hertog, Noonan and LEOPARD syndrome Shp2 variants induce heart displacement defects in zebrafish. *Development* **141**, 1961–1970 (2014).
42. Y. Goyal, G. A. Jindal, J. L. Pelliccia, K. Yamaya, E. Yeung, A. S. Futran, R. D. Burdine, T. Schüpbach, S. Y. Shvartsman, Divergent effects of intrinsically active MEK variants on developmental Ras signaling. *Nat. Genet.* **49**, 465–469 (2017).
43. G. A. Jindal, Y. Goyal, J. M. Humphreys, E. Yeung, K. Tian, V. L. Patterson, H. He, R. D. Burdine, E. J. Goldsmith, S. Y. Shvartsman, How activating mutations affect MEK1 regulation and function. *J. Biol. Chem.* **292**, 18814–18820 (2017).
44. G. A. Jindal, Y. Goyal, K. Yamaya, A. S. Futran, I. Kountouridis, C. A. Balgobin, T. Schüpbach, R. D. Burdine, S. Y. Shvartsman, In vivo severity ranking of Ras pathway mutations associated with developmental disorders. *Proc. Natl. Acad. Sci. U.S.A.* **114**, 510–515 (2017).
45. E. Kague, M. Gallagher, S. Burke, M. Parsons, T. Franz-Odendaal, S. Fisher, Skeletogenic fate of zebrafish cranial and trunk neural crest. *PLOS ONE* **7**, e47394 (2012).
46. C. J. Huang, C. T. Tu, C. D. Hsiao, F. J. Hsieh, H. J. Tsai, Germ-line transmission of a myocardium-specific GFP transgene reveals critical regulatory elements in the cardiac myosin light chain 2 promoter of zebrafish. *Dev. Dyn.* **228**, 30–40 (2003).
47. E. Esen, I. Sergin, R. Jesudason, P. Himmels, J. D. Webster, H. Zhang, M. Xu, R. Piskol, E. McNamara, S. Gould, A. H. Capietto, L. Delamarre, K. Walsh, W. Ye, MAP4K4 negatively regulates CD8 T cell-mediated antitumor and antiviral immunity. *Sci. Immunol.* **5**, eaay2245 (2020).
48. Y. Zhang, Y. Li, Q. Wang, B. Su, H. Xu, Y. Sun, P. Sun, R. Li, X. Peng, J. Cai, Role of RASA1 in cancer: A review and update. *Oncol. Rep.* **44**, 2386–2396 (2020).
49. S. Richards, N. Aziz, S. Bale, D. Bick, S. das, J. Gastier-Foster, W. W. Grody, M. Hegde, E. Lyon, E. Spector, K. Voelkerding, H. L. Rehm; ACMG Laboratory Quality Assurance Committee, Standards and guidelines for the interpretation of sequence variants: a joint consensus recommendation of the American College of Medical Genetics and Genomics and the Association for Molecular Pathology. *Genet. Med.* **17**, 405–424 (2015).
50. J. Schottenfeld, J. Sullivan-Brown, R. D. Burdine, Zebrafish curly up encodes a Pkd2 ortholog that restricts left-side-specific expression of southpaw. *Development* **134**, 1605–1615 (2007).
51. S. Yuan, Z. Sun, Microinjection of mRNA and morpholino antisense oligonucleotides in zebrafish embryos. *J. Vis. Exp.* , 1113 (2009).
52. M. Isrie, M. Breuss, G. Tian, A. H. Hansen, F. Cristofoli, J. Morandell, Z. A. Kupchinsky, A. Sifrim, C. M. Rodriguez-Rodriguez, E. P. Dapena, K. Doonanco, N. Leonard, F. Tinsa, S. Moortgat, H. Ulucan, E. Koparir, E. Karaca, N. Katsanis, V. Marton, J. R. Vermeesch, E. E. Davis, N. J. Cowan, D. A. Keays, H. van Esch, Mutations in either TUBB or MAPRE2 cause circumferential skin creases kunze type. *Am. J. Hum. Genet.* **97**, 790–800 (2015).

Acknowledgments: We thank all the individuals and their families who took part in this study. We thank P. Johnson for zebrafish husbandry and J. K. Holsclaw for technical assistance with zebrafish knockdown experiments. We also thank M. Li for Sanger sequencing analysis. **Funding:** This work was supported by National Institute of Child Health and Human Development R03HD092694 (R.D.B. and E.B.), K23HD088742 (N.L.V.), R01HD105868 (N.L.V. and E.E.D.), and R01HD055651-11 (K.W.); National Institute of General Medical Sciences R01GM086537 (R.D.B.); National Institute of Arthritis and Musculoskeletal and Skin Diseases R01AR071486 (R.D.B.); National Center for Advancing Translational Sciences R21TR002770 (N.L.V. and E.E.D.); National Institute of Mental Health grant R01MH106826 (E.E.D.); National Human Genome Research Institute U01HG006487-05 (K.W.); and Duke/UNC CTSA Consortium Collaborative Translational Research Grant DUR41703-UL1TR002553. Research from V.P. and R.D.B. reported in this publication was supported by the New Jersey Health Foundation Inc. under award number PC 59-20 and by the National Institute of Arthritis and Musculoskeletal and Skin Diseases of the National Institutes of Health under award number R01AR071486. The content is solely the responsibility of the authors and does not necessarily represent the official views of the National Institutes of Health. **Author contributions:** Conceptualization: V.P., D.L., R.D.B., E.B., J.N.G., and E.E.D. Investigation: V.P., F.U., D.L., J.N.G., K.W., F.T.M.-T., A.R., A.A., V.S., M.Mi., T.G., J.H., M.W., K.M.R., B.S., K.G., B.C.P., L.B., A.S., S.S., M.B., M.S.S., R.S., S.E., D.K.G., X.H., Y.L., Y.S., M.Mu., E.Z., A.R., K.I., J.H., N.H.R., D.G., C.M., B.K., H.C., J.J., M.H., C.F.G., A.V., A.-L.B., A.S., S.M., F.L.R., K.G., B.C.P., K.W., C.L., A.T.V.-v.S., T.G., M.M.M., A.A., V.S., F.Z., N.L.V., E.E.D., R.D.B., and E.J.B. Visualization: V.P., E.B., F.U., and E.E.D. Supervision: R.D.B., E.B., E.E.D., and N.L.V. Writing (original draft): V.P. Writing (review and editing): R.D.B., E.B., F.U., D.L., J.N.G., E.E.D., N.L.V., K.W., A.S., S.S., D.K.G., A.R., A.A., V.S., J.H., M.W., K.M.R., and B.S. **Competing interests:** E.E.D. is the Ann Marie and Francis Klocke, MD Research Scholar. All authors declare that they have no other competing interests. **Data and materials availability:** All data needed to evaluate the conclusions in the paper are present in the paper and/or the Supplementary Materials. All variants have been deposited into ClinVar, accession number VCV001804004.1, with appropriate annotation.

Submitted 21 July 2022
Accepted 24 March 2023
Published 26 April 2023
10.1126/sciadv.ade0631